Anomalous phonon Grüneisen parameters in the semiconductor Ta$_2$NiS$_5$

Mai Ye [1,*] Tom Lacmann,[1] Mehdi Frachet [1,†] Igor Vinograd [1,‡] Gaston Garbarino,[2] Nour Maraytta [1]
Michael Merz [1,3] Rolf Heid [1] Amir-Abbas Haghighirad [1] and Matthieu Le Tacon [1,§]

[1]*Institute for Quantum Materials and Technologies, Karlsruhe Institute of Technology, Kaiserstrasse 12, 76131 Karlsruhe, Germany*
[2]*European Synchrotron Radiation Facility, BP 220, F-38043 Grenoble Cedex, France*
[3]*Karlsruhe Nano Micro Facility (KNMFi), Karlsruhe Institute of Technology, Kaiserstrasse 12, 76131 Karlsruhe, Germany*

Strain tuning is a powerful experimental method in probing correlated electron systems. Here we study the strain response of the lattice dynamics and electronic structure in the semiconductor Ta$_2$NiS$_5$ by polarization-resolved Raman spectroscopy. We observe an increase of the size of the direct semiconducting band gap. Although the majority of the optical phonons show only marginal dependence to applied strain, the frequency of the two B$_{2g}$ phonon modes, which have quadrupolar symmetry and already anomalously soften on cooling under zero strain, increases significantly with tensile strain along the *a* axis. The corresponding Grüneisen parameters are unusually large in magnitude and negative in sign. These effects are well captured by first-principles density functional theory calculations and indicate close proximity of Ta$_2$NiS$_5$ to a structural instability, similar to that encountered in excitonic insulator candidate Ta$_2$NiSe$_5$.

I. INTRODUCTION

A macroscopic number of bound pairs of fermions, formed at low temperatures due to attractive interaction, result in quantum phases with superconductivity [1] or superfluidity [2]. Excitonic insulators (EIs) belong to such quantum phases, in that the Coulomb attraction in a semimetal or in a narrow-gap semiconductor leads to an instability toward the formation of electron-hole pairs (excitons) [3–5] and these bosonic quasiparticles can collectively establish a coherent state and open an interaction-induced gap [6]. Furthermore, if the participating electron and hole states belong to bands of different symmetry, then the resulting EI breaks the crystal lattice symmetry.

The material family Ta$_2$Ni(Se$_{1-x}$S$_x$)$_5$ serves as a suitable platform to investigate the rich physics of EIs. On one end of its phase diagram, Ta$_2$NiSe$_5$ is largely believed to be a semimetal at high temperature [7,8] which has been proposed to host an EI state [9] below an orthorhombic-to-monoclinic structural phase transition around 326 K [10,11]. This transition reduces the point-group symmetry from D_{2h} to C_{2h} by breaking two mirror symmetries, and by group theory the corresponding order parameter is of B$_{2g}$ symmetry. It is accompanied with the opening of a gap in the electronic dispersion and a band flattening [9], but there is generally a controversy on whether these features can be effectively attributed to the condensation of excitons [12–16], or they

are only a consequence of the lattice symmetry lowering and electron-phonon coupling [7,17,18].

The transition temperature is suppressed by S substitution [11,19,20], and at the other end of the phase diagram, the isostructural compound Ta$_2$NiS$_5$ is a semiconductor with a band gap exceeding the exciton binding energy, henceforth forbidding the EI instability [10,21,22]. In contrast with Ta$_2$NiSe$_5$, the properties of semiconducting Ta$_2$NiS$_5$ have been relatively little explored. It is for instance unclear whether the aforementioned structural transition is completely suppressed. This has been suggested in recent x-ray diffraction experiments [22], but Raman scattering investigation [20] has interpreted a temperature-dependent breaking of the phonon polarization selection rules below 120 K as evidence for such transition. This view is further supported by first-principles calculations [23] indicating that in both Ta$_2$NiSe$_5$ and Ta$_2$NiS$_5$, the lattice symmetry is broken by phonon instabilities, emphasizing the importance of lattice degrees of freedom in shaping the phase diagram of this family of materials.

In this work, we tackle this issue from a different perspective, probing the response of the phononic and electronic degrees of freedom of Ta$_2$NiS$_5$ to uniaxial strain. Strain tuning has proven particularly insightful in studying the electronic properties of unconventional low- [24,25] or high-temperature superconductors [26–28], ferromagnets [29], antiferromagnets [30], and topological systems [31]. Here we combine it with Raman spectroscopy and first-principles calculations to reveal the highly anomalous behavior of two phonon modes of B$_{2g}$ symmetry involving shear vibrations of the Ta atoms along the crystallographic *a* direction. We show that this behavior arises independently from changes of the band gap size and points toward an intrinsic structural instability of the orthorhombic unit cell upon volume reduction. More generally, our results demonstrate the possibility of manipulating

*Contact author: mai.ye@kit.edu

†Present address: CEA-Leti, Université Grenoble Alpes, Grenoble, France.

‡Present address: 4th Physical Institute–Solids and Nanostructures, University of Göttingen, 37077 Göttingen, Germany.

§Contact author: matthieu.letacon@kit.edu

the electronic band gap in the $Ta_2Ni(Se_{1-x}S_x)_5$ family using strain, which offers interesting perspectives to approach the still elusive EI regime.

II. METHOD

High-quality single crystals of Ta_2NiS_5 were grown using chemical vapor transport [32]. The composition of the obtained crystals was performed using energy dispersive x-ray spectroscopy (EDX) in a COXEM EM-30plus electron microscope equipped with an Oxford silicon-drift-detector (SDD) and AZtecLiveLite software package.

Strain-dependent Raman-scattering experiments were performed with a Horiba Jobin-Yvon LabRAM HR evolution spectrometer. We used a He-Ne laser (632.8 nm) with less than 1 mW power that was focused on the sample with a ×50 magnification objective. The laser spot size was around 5 μm in diameter. One notch filter and two Bragg filters were used in the collection optical path to filter the elastically scattered light. Spectra were recorded with 1800 mm^{-1} (0.6 cm^{-1} spectral resolution) and 600 mm^{-1} (1.6 cm^{-1} spectral resolution) gratings and a liquid-nitrogen-cooled CCD detector. All spectra of Raman response were corrected for the instrumental spectral response and Bose factor. Two polarization configurations were employed to probe excitations in different symmetry channels, namely the *aa* and *ac* configurations in which the incident light polarization lies along the crystallographic *a* direction, and scattered one along *a* or *c* direction, respectively. According to Raman selection rules [33], in the orthorhombic phase (point group D_{2h}), the *aa* and *ac* geometries probe the A_g and B_{2g} Raman signal, respectively. Samples with a cleaved crystallographic *ac* plane were glued to Razorbill CS220T strain cell by Loctite Stycast 2850FT epoxy with CAT 24LV as the epoxy catalyst. The sample surfaces were examined under polarized light to find an area without intrinsic strain. We verified that the process of mounting the sample onto the strain cell does not introduce additional stress by comparing the Raman spectra of unmounted and mounted samples. The strain transmission was estimated from XRD measurement as detailed in the supplemental material [32]; the corresponding data measured at European Synchrotron Radiation Facility (ESRF) ID15B beamline are available from the ESRF Data Portal [34].

Density functional theory (DFT) calculations were performed using the mixed-basis pseudopotential method [35] to assess the effect of uniaxial strain on the electronic structure and Raman active modes [32]. The exchange-correlation functional was represented by the generalized gradient approximation (GGA) [36]. The DFT + U approach was applied with $U = 10$ eV for the Ni d states. We performed all calculations in the room-temperature orthorhombic structure (space group *Cmcm*). Lattice constants were taken from Sunshine *et al.* [37], $a = 3.415$ Å, $b = 12.146$ Å, $c = 15.097$ Å. The relatively small tensile strain was modeled by scaling *a* only, ignoring any elastic reaction of the *b* or *c* axes. For each structure, atomic positions were relaxed until forces were smaller than 2.6 meV/Å. Raman-mode frequencies were calculated using the linear response, or density-functional perturbation theory (DFPT), implemented in the mixed-basis pseudopotential method [38].
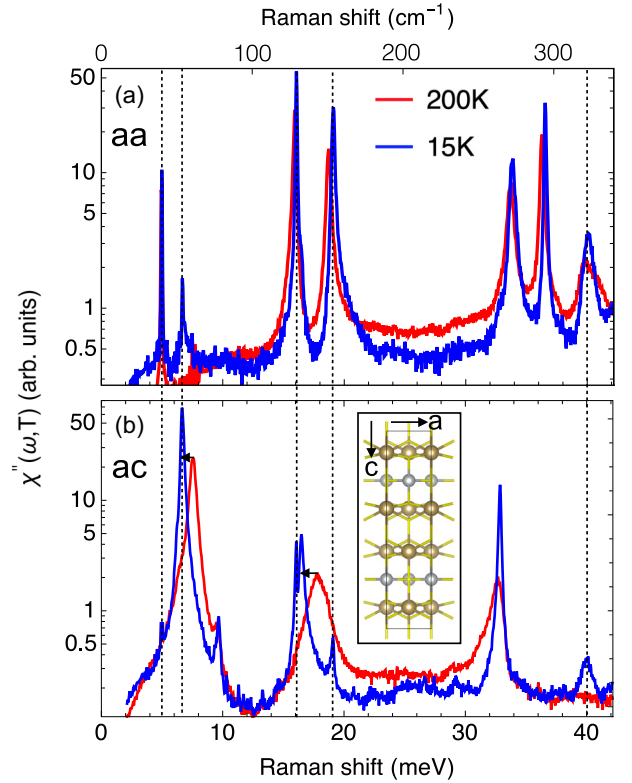

FIG. 1. Log-scale Raman response χ'' in the *aa* (a) and *ac* (b) scattering geometry, respectively. The corresponding light polarizations are illustrated at top left of each panel. The spectral features of phonon-mode "leakage" are labeled by dashed vertical lines. The anomalous softening of the two lowest-energy B_{2g} phonons is labeled by solid horizontal arrows in panel (b). The inset in panel (b) is a sketch of the crystal structure with the a- and c-axes labeled. The tantalum atoms are shown in brown and the nickel atoms are shown in grey. The sulfur atoms are omitted for clarity.

III. RESULTS AND DISCUSSION

A. Strain-free phonon spectra

In agreement with previous Raman-scattering investigation [20], we observe a "leakage" of certain phonon modes at low temperatures. This is illustrated by the Raman spectra measured at 200 and 15 K in two configurations, as shown in Fig. 1. Up to 40 meV, and in agreement with the selection rules of the orthorhombic phase, six A_g Raman phonons are observed in the *aa* scattering geometry and three B_{2g} modes in the *ac* scattering geometry. At low temperature, on the contrary, the lowest-energy B_{2g} mode becomes apparent ("leaks") in the *aa* scattering geometry, breaking down the aforementioned selection rules. Similarly, four A_g modes "leak" in the spectra recorded in the *ac* scattering geometry at low temperature. Such leakage strongly suggests a reduction of the D_{2h} point group symmetry of the orthorhombic phase and, akin to Ta_2NiSe_5 [10], the most natural point group candidate would correspond to a monoclinic C_{2h} phase that breaks the $m_a(a \rightarrow -a)$ and $m_c(c \rightarrow -c)$ mirror symmetries.

The phonon leakage is an indication of symmetry breaking, and the phonon softening suggests a tendency toward an orthorhombic-to-monoclinic structural distortion. A recent

XRD experiment finds no clear evidence for a structural transition [22]. Our in-house XRD investigation could not reveal any signature of such transition down to 80 K [32] and our refinement of the crystal structure of Ta_2NiS_5 at 15 K with data taken at the synchrotron is not yet fully conclusive [32]. As a result additional studies are called for to clarify this issue.

Nonetheless, another noteworthy feature of the Raman spectra of Ta_2NiS_5 is the anomalous softening of the two lowest-energy B_{2g} modes (hereafter labeled $B_{2g}^{(1)}$ and $B_{2g}^{(2)}$) on cooling. As previously noted [20], this behavior is inconsistent with the conventional anharmonic decay of phonons in solids and might indicate the proximity of a phase transition. Because of the lattice contraction upon cooling, the corresponding Grüneisen parameter $\gamma_i = -(\Delta\omega_i/\omega_i)/(\Delta V/V)$ of these phonons is negative, which indicates that the orthorhombic structure is generally unstable against a reduction of the unit cell volume. Interestingly, the order parameter of the orthorhombic-to-monoclinic transition in Ta_2NiSe_5 has the B_{2g} symmetry and the vibration pattern of the two lowest-energy B_{2g} modes, which couple to the overdamped excitonic mode [19], consists of a shear displacement of the Ta along the a direction, reminiscent of the structural distortion (in contrast with the $B_{2g}^{(3)}$ mode which involves mostly S vibrations and behaves normally). Nevertheless, the relevant B_{2g} modes in Ta_2NiSe_5 exhibit no softening behavior [19,20], consistent with the view that the transition is driven by an excitonic instability. Taken together, these observations indicate that lattice strain tuning might be a promising tuning knob of the electronic properties of this system, as discussed below.

B. Strain-dependent Raman spectra

Next, we investigate the strain response of the system. Because of the anisotropic structure of Ta_2NiS_5, and the fact that the putative structural distortion of the material is of B_{2g} symmetry which transforms as an ac quadrupole, we choose to focus on the spectral response of tensile strain along the crystallographic a direction, which is also favoured by the morphology of the single crystals.

In Fig. 2, we show the phonon spectra measured at 15 K as function of a-axis tensile strain up to 0.25%. As previously explained, in the monoclinic phase, all the modes observed in aa [Fig. 2(a)] or ac [Fig. 2(b)] configurations have the A_g symmetry of C_{2h} group. However, we observe a clear qualitative difference of the strain response for the modes which have larger intensity in the aa configuration (which had the A_g symmetry of D_{2h} group in the high-temperature orthorhombic phase) and those seen in the ac scattering geometry that had B_{2g} character at high temperature. For clarity, we continue to label these phonons according to their high temperature symmetry. Strikingly, the $B_{2g}^{(1)}$ and $B_{2g}^{(2)}$ harden significantly and their lineshape narrows with increasing tensile strain [insets of Fig. 2(b)]. This behavior starkly contrast with the behavior of the $B_{2g}^{(3)}$ mode or with the observation in the aa configuration, where we can barely detect a change in the frequency or linewidth of the A_g phonons in the investigated strain range.

To quantify the magnitude of these effects, we have fitted the different modes using standard Lorentzian lineshape. The strain dependence of the frequency and linewidth at 15 K for the three B_{2g} phonon modes are shown in Figs. 3(a)–3(c).
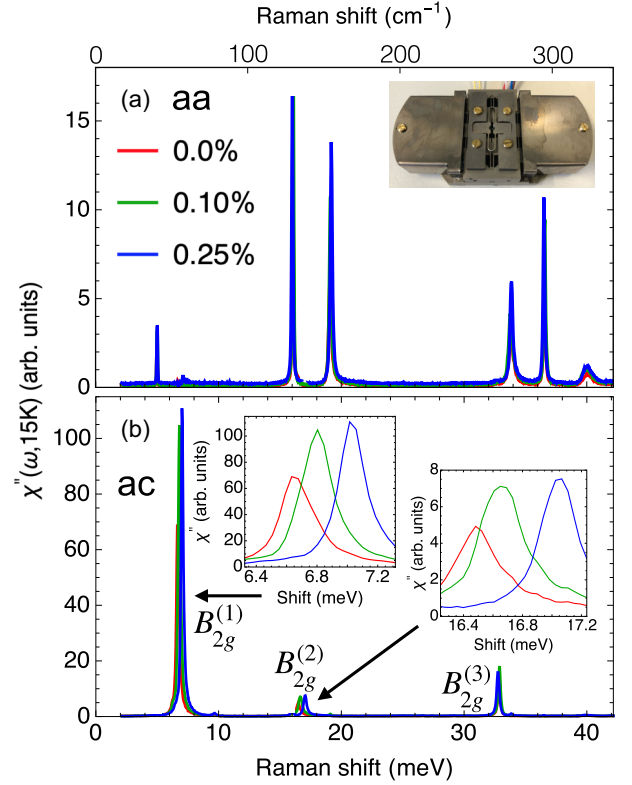

FIG. 2. Raman response χ'' measured under various a axis tensile strain at 15 K in the (a) aa and (b) ac scattering geometries. The inset in panel (a) exhibits the Razorbill strain cell CS220T used for the Raman experiments. The insets in panel (b) show the strain dependence of the two lowest-frequency B_{2g}-symmetry phonon modes.
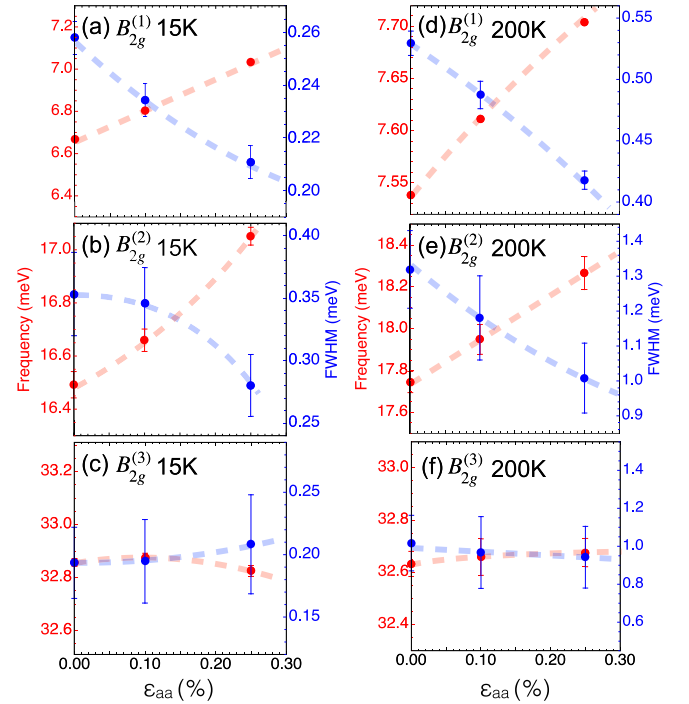

FIG. 3. Tensile strain (ϵ_{aa}) dependence of the frequency and full width at half maximum (FWHM) for the three B_{2g} phonon modes at 15 K [(a)–(c)] and 200 K [(d)–(f)]. The dashed lines are a guide to the eyes.

With 0.25% strain, the relative frequency shift for the $B_{2g}^{(1)}$, $B_{2g}^{(2)}$, and $B_{2g}^{(3)}$ modes are 5.5, 3.4, and 0.1%, respectively. The relative frequency changes for the A_g modes are all less than 0.5%. Besides the significant hardening of frequency, the $B_{2g}^{(1)}$ and $B_{2g}^{(2)}$ modes exhibit a 20% reduction of linewidth. This effect is completely absent for the other modes, whose linewidth is nearly strain-independent. The behaviors of the linewidth demonstrate that within the probed volume the strain is homogeneous, because inhomogeneity would result in lineshape broadening [39].

The relative frequency change, 5.5% and 3.4%, of the two lowest-energy B_{2g} phonon modes at 0.25% strain is anomalously large compared to other systems. To fix ideas regarding the amplitude of this effect, we provide hereafter a few examples from the recent literature for comparison. We first consider the silicon T_{2g}-symmetry phonon mode which has a frequency of around 520 cm^{-1}. Under as large as 8.5% strain induced in silicon membranes by ion implantation, the magnitude of the relative frequency change is 4.9% [40], which is in between the values 5.5% and 3.4% we found. We then consider some two-dimensional systems whose strain response is actively studied [41]. The phonon modes of monolayer transition-metal-dichalcogenides WSe_2 and WS_2 only show around 2% frequency shift at 2.85% tensile strain [39], and CrSBr flake exhibits about 2% frequency change at 1.7% tensile strain [42]. These ratios between the frequency change and strain are closer to the strain effect observed for the A_g phonon modes of Ta_2NiS_5, and generally expected from Grüneisen's law, with Grüneisen parameters of individual phonons lying in the range of a few units for most systems semiconductor and metallic systems [43]. Here and in agreement with the temperature dependent experiment discussed in the previous section, the Grüneisen parameters for the $B_{2g}^{(1)}$ and $B_{2g}^{(2)}$ phonon modes in Ta_2NiS_5 are not only much larger in magnitude but also anomalously negative, reaching -22 and -13.6, respectively.

To find out whether the anomalous behavior of the $B_{2g}^{(1)}$ and $B_{2g}^{(2)}$ modes could be related to strain-induced changes in the electronic structure, we also studied the strain-dependence of the electronic excitations. As previously reported [19], the presence of a direct semiconducting gap suppresses every low-energy electronic excitation in Ta_2NiS_5. The lowest interband transition manifests itself already at 200 K in the form of a broad excitation centered around 300 meV [Fig. 4(b)]. At 15 K, the spectrum sharpens significantly and the overall profile changes [Fig. 4(a)]. We do not see the B_{2g}-symmetry exciton mode as clearly sharp and strong as in Ref. [19], presumably because of the narrow resonance profile of this feature (our measurement is performed with 633 nm laser excitation rather than with 647 nm line used in Ref. [19]). The spectra are however perfectly consistent with previous reports, showing as well a weaker spectral feature at around 330 meV, which has previously been interpreted as the second state of the Rydberg series [19]. Under applied *a*-axis stress, a continuous hardening of the electronic excitation spectra arises both at high and low temperatures. With 0.25% strain, a relative blue shift of the excitation spectra amounting to 4.3% (from 302 to 315 meV) is observed. This 4.3% change of band
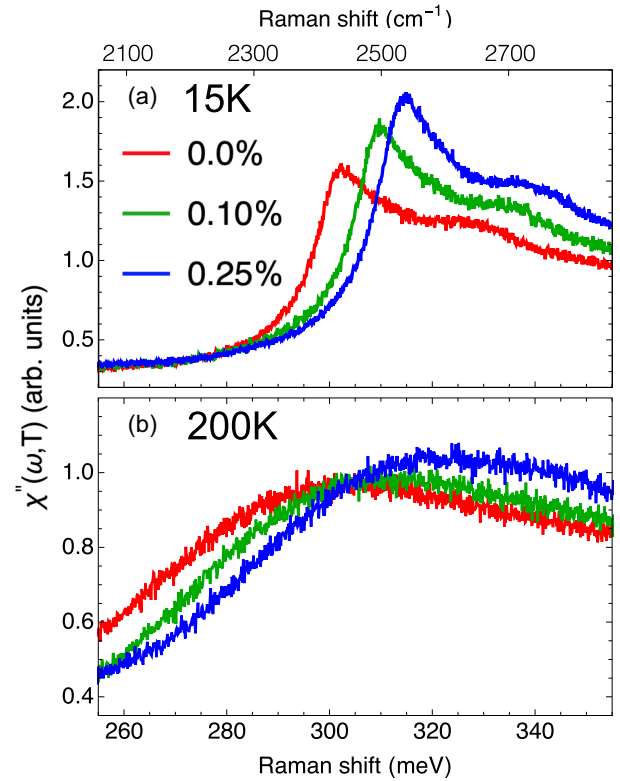

FIG. 4. High-energy Raman response χ'' measured under various *a* axis tensile strain at (a) 15 K and (b) 200 K in the *ac* scattering geometry.

gap at 0.25% strain is now well comparable to the behaviors encountered in other semiconducting systems such as bilayer MoS_2 under tensile strain [44], or trilayer MoS_2 under various biaxial compressive strains [45]. Qualitatively, we can associate this behavior with a reduction, under tensile strain along the crystallographic *a* direction, of the overlap between Ta 5d orbitals (so their hybridization), on the one hand, and between the Ni 3d orbitals, on the other hand, which yields an overall reduction of the bandwidth of the respective bands across the direct semiconducting gap, naturally yielding its increase. At the same time, the concomitant anomalous hardening of the two $B_{2g}^{(1)}$ and $B_{2g}^{(2)}$ phonon frequencies indicates an increased stability of the structure at larger unit cell volumes, hinting toward an intrinsic structural instability of the shrunk unit cell (e.g., under the effect of cooling).

C. First-principles calculations and discussion

To gain further insights, it is instructive to compare our experimental results with those from first principle calculations. In Table I, we compare the experimentally measured energy of three optical phonon modes and the band gap with the calculated values (note that experimental lattice parameters are used for the calculation [32]). Interestingly, within our computational approach, the eigenvalue of the dynamical matrix for the $B_{2g}^{(1)}$ mode is imaginary, and the structure therefore unstable against the eigendisplacement of this mode, which precisely involve the shear motion of the Ta ions along the a axis that would yield a monoclinic distortion akin to the Se

TABLE I. Comparison between the experimentally measured (Exp.) energy values and the calculated (Cal.) ones for selected phonon modes and band gap at 15 K. The $A_{1g}^{(1)}$ mode refers to the A_{1g} phonon with the lowest energy. The experimentally measured band gap is defined as the energy at which the interband excitations have the maximal intensity; the calculated value corresponds to a direct gap at Γ point. The values in the brackets give the change compared to the corresponding zero-strain value. The unit for energies is meV.

Strain	0%		0.1%		0.25%	
	Exp.	Cal.	Exp.	Cal.	Exp.	Cal.
Gap	302	126	309	132	315	146
			(+7)	(+7)	(+13)	(+20)
$A_{1g}^{(1)}$	4.99	4.79	5.01	4.78	5.01	4.81
			(+.02)	(-.01)	(+.00)	(+.02)
$B_{2g}^{(2)}$	16.49	15.18	16.66	15.41	17.05	15.73
			(+.17)	(+.23)	(+.56)	(+.55)
$B_{2g}^{(3)}$	32.86	32.46	32.87	32.50	32.83	32.49
			(+.01)	(+.04)	(-.03)	(+.03)

compound. Leaving this aside, we can look at the electronic structure. As discussed in the Supplemental Material [32] and in agreement with previous computational work [23], correlation corrections for the Ni d states need to be introduced in the framework of the GGA + U approach to open a direct semiconducting gap in the electronic structure. A 126 meV gap is obtained for $U = 10$ eV, which is significantly lower than the experimental value indicating that nonlocal self energy effects, especially that of Ta and Ni orbitals near the Fermi level, should be taken into account to reproduce the realistic band gap [23]. Nevertheless, the relative magnitude of the strain-induced effects on the gap is correctly captured by our calculation, validating the qualitative picture drawn earlier.

We also find that the calculated energy of the phonon modes is in good agreement with the experimental values, and the absolute renormalization of the $B_{2g}^{(2)}$ frequency with strain as well as the absence of renormalization for the $A_{1g}^{(1)}$ and $B_{2g}^{(3)}$ (and so essentially their respective Grüneisen parameters) are perfectly captured by the calculation. As already emphasized, the $B_{2g}^{(2)}$ (and $B_{2g}^{(1)}$) mode involves a shear motion of Ta ions along a, a pattern that was previously found theoretically to strongly modulate the semiconducting gap size [23]. This raises the question to know whether the anomalous behavior of this mode should then be attributed to the strain-induced change of the semiconducting gap, or whether it rather arises only from lattice stretching.

To address this, we can evaluate the relative contributions to the energy shifts from the change of lattice structure and

gap by comparing the results obtained with different strains but identical gaps (by adjusting U). In Table II, we show that with 1.0% strain and $U = 7$ eV, the gap size is comparable to the value obtained with 0.1% strain and $U = 10$ eV (Table I), but 36% smaller than the value obtained with 1.0% strain and $U = 10$ eV. In agreement with previous discussion, we find that changes in U, strain and gap size affect only marginally the $B_{2g}^{(3)}$ and A_{1g}-symmetry phonon mode frequencies. However, the 36% gap size reduction yields a 4% softening of the $B_{2g}^{(2)}$ mode, whereas the decrease of strain from 1% to 0.1% with constant gap value yields a comparatively larger softening of 10% frequency of the $B_{2g}^{(2)}$ phonon frequency.

From these discussions we see that the anomalous behavior of the $B_{2g}^{(2)}$ phonon, both as function of temperature and of strain, is rooted in an incipient instability of the orthorhombic lattice structure against a shear monoclinic distortion of the Ta chains, which is likely to occur irrespective of the electronic gap size. Time-resolved spectroscopy, which has been successfully used in the study of Ta_2NiSe_5 to disentangle the charge and lattice dynamics [16,17,46–48], would provide further support to this view.

Although additional work is required to examine whether this distortion is effectively realized in Ta_2NiS_5, as suggested by the Raman data, our work demonstrates that the susceptibility toward it is very large, and would likely occur upon compression of the lattice. At the same time, such a perturbation would allow a reduction of the semiconducting gap size, which would offer an interesting way to approach the regime in which an EI can occur (i.e., when the gap size becomes lower than the exciton binding energy).

IV. CONCLUSION

In summary, we have used polarization-resolved Raman spectroscopy to study the response of phononic and electronic degrees of freedom to uniaxial strain in Ta_2NiS_5. In particular, we found that tensile strain along the a axis results in an anomalously large frequency increase for two B_{2g} phonon modes. The corresponding Grüneisen parameter for the lowest-energy B_{2g} mode is negative and has an magnitude larger than 20. DFT calculations support that such anomalous Grüneisen parameter results from a proximity to a structural instability similar to the one in excitonic insulator candidate Ta_2NiSe_5. Besides, the band gap of this system increases with strain, as the tensile strain reduces the orbital overlap and in turn the bandwidth. These experimental results establish Ta_2NiS_5 as a suitable platform to explore strain tuning of lattice dynamics and electronic structure.

TABLE II. Comparison between the calculated energy values for the B_{2g} phonon modes and band gap under 1.0% strain.

	Gap	$B_{2g}^{(2)}$	$B_{2g}^{(3)}$
$U = 10$ eV	213.5 meV	17.21 meV	32.40 meV
$U = 7$ eV	136.7 meV	16.50 meV	32.48 meV
Relative change	−36.0%	−4.1%	+0.2%

[1] J. Bardeen, L. N. Cooper, and J. R. Schrieffer, Theory of superconductivity, Phys. Rev. **108**, 1175 (1957).

[2] P. W. Anderson, *Basic Notions of Condensed Matter Physics* (CRC Press, Boca Raton, FL, 1994).

[3] W. Kohn, Excitonic phases, Phys. Rev. Lett. **19**, 439 (1967).

[4] D. Jérome, T. M. Rice, and W. Kohn, Excitonic insulator, Phys. Rev. **158**, 462 (1967).

[5] B. I. Halperin and T. M. Rice, Possible anomalies at a semimetal-semiconductor transition, Rev. Mod. Phys. **40**, 755 (1968).

[6] W. Kohn and D. Sherrington, Two kinds of bosons and Bose condensates, Rev. Mod. Phys. **42**, 1 (1970).

[7] M. D. Watson, I. Marković, E. A. Morales, P. Le Fèvre, M. Merz, A. A. Haghighirad, and P. D. C. King, Band hybridization at the semimetal-semiconductor transition of Ta_2NiSe_5 enabled by mirror-symmetry breaking, Phys. Rev. Res. **2**, 013236 (2020).

[8] P. A. Volkov, M. Ye, H. Lohani, I. Feldman, A. Kanigel, and G. Blumberg, Critical charge fluctuations and emergent coherence in a strongly correlated excitonic insulator, npj Quantum Mater. **6**, 52 (2021).

[9] Y. Wakisaka, T. Sudayama, K. Takubo, T. Mizokawa, M. Arita, H. Namatame, M. Taniguchi, N. Katayama, M. Nohara, and H. Takagi, Excitonic insulator state in Ta_2NiSe_5 probed by photoemission spectroscopy, Phys. Rev. Lett. **103**, 026402 (2009).

[10] F. D. Salvo, C. Chen, R. Fleming, J. Waszczak, R. Dunn, S. Sunshine, and J. A. Ibers, Physical and structural properties of the new layered compounds Ta_2NiS_5 and Ta_2NiSe_5, J. Less-Common Met. **116**, 51 (1986).

[11] Y. F. Lu, H. Kono, T. I. Larkin, A. W. Rost, T. Takayama, A. V. Boris, B. Keimer, and H. Takagi, Zero-gap semiconductor to excitonic insulator transition in Ta_2NiSe_5, Nat. Commun. **8**, 14408 (2017).

[12] T. Kaneko, T. Toriyama, T. Konishi, and Y. Ohta, Orthorhombic-to-monoclinic phase transition of Ta_2NiSe_5 induced by the Bose-Einstein condensation of excitons, Phys. Rev. B **87**, 035121 (2013).

[13] K. Seki, Y. Wakisaka, T. Kaneko, T. Toriyama, T. Konishi, T. Sudayama, N. L. Saini, M. Arita, H. Namatame, M. Taniguchi, N. Katayama, M. Nohara, H. Takagi, T. Mizokawa, and Y. Ohta, Excitonic Bose-Einstein condensation in Ta_2NiSe_5 above room temperature, Phys. Rev. B **90**, 155116 (2014).

[14] G. Mazza, M. Rösner, L. Windgätter, S. Latini, H. Hübener, A. J. Millis, A. Rubio, and A. Georges, Nature of symmetry breaking at the excitonic insulator transition: Ta_2NiSe_5, Phys. Rev. Lett. **124**, 197601 (2020).

[15] K. Fukutani, R. Stania, C. Il Kwon, J. S. Kim, K. J. Kong, J. Kim, and H. W. Yeom, Detecting photoelectrons from spontaneously formed excitons, Nat. Phys. **17**, 1024 (2021).

[16] K. Katsumi, A. Alekhin, S.-M. Souliou, M. Merz, A.-A. Haghighirad, M. Le Tacon, S. Houver, M. Cazayous, A. Sacuto, and Y. Gallais, Disentangling lattice and electronic instabilities in the excitonic insulator candidate Ta_2NiSe_5 by nonequilibrium spectroscopy, Phys. Rev. Lett. **130**, 106904 (2023).

[17] E. Baldini, A. Zong, D. Choi, C. Lee, M. H. Michael, L. Windgaetter, I. I. Mazin, S. Latini, D. Azoury, B. Lv, A. Kogar, Y. Su, Y. Wang, Y. Lu, T. Takayama, H. Takagi, A. J. Millis, A. Rubio, E. Demler, and N. Gedik, The spontaneous symmetry breaking in Ta_2NiSe_5 is structural in nature, Proc. Natl. Acad. Sci. USA **120**, e2221688120 (2023).

[18] C. Chen, X. Chen, W. Tang, Z. Li, S. Wang, S. Ding, Z. Kang, C. Jozwiak, A. Bostwick, E. Rotenberg, M. Hashimoto, D. Lu, J. P. C. Ruff, S. G. Louie, R. J. Birgeneau, Y. Chen, Y. Wang, and Y. He, Role of electron-phonon coupling in excitonic insulator candidate Ta_2NiSe_5, Phys. Rev. Res. **5**, 043089 (2023).

[19] P. A. Volkov, M. Ye, H. Lohani, I. Feldman, A. Kanigel, and G. Blumberg, Failed excitonic quantum phase transition in $Ta_2Ni(Se_{1-x}S_x)_5$, Phys. Rev. B **104**, L241103 (2021).

[20] M. Ye, P. A. Volkov, H. Lohani, I. Feldman, M. Kim, A. Kanigel, and G. Blumberg, Lattice dynamics of the excitonic insulator $Ta_2Ni(Se_{1-x}S_x)_5$, Phys. Rev. B **104**, 045102 (2021).

[21] Y. Chiba, T. Mitsuoka, N. L. Saini, K. Horiba, M. Kobayashi, K. Ono, H. Kumigashira, N. Katayama, H. Sawa, M. Nohara, Y. F. Lu, H. Takagi, and T. Mizokawa, Valence-bond insulator in proximity to excitonic instability, Phys. Rev. B **100**, 245129 (2019).

[22] C. Chen, W. Tang, X. Chen, Z. Kang, S. Ding, K. Scott, S. Wang, Z. Li, J. P. C. Ruff, M. Hashimoto, D.-H. Lu, C. Jozwiak, A. Bostwick, E. Rotenberg, E. H. da Silva Neto, R. J. Birgeneau, Y. Chen, S. G. Louie, Y. Wang, and Y. He, Anomalous excitonic phase diagram in band-gap-tuned $Ta_2Ni(Se, S)_5$, Nat. Commun. **14**, 7512 (2023).

[23] L. Windgätter, M. Rösner, G. Mazza, H. Hübener, A. Georges, A. J. Millis, S. Latini, and A. Rubio, Common microscopic origin of the phase transitions in Ta_2NiS_5 and the excitonic insulator candidate Ta_2NiSe_5, npj Comput. Mater. **7**, 210 (2021).

[24] C. W. Hicks, D. O. Brodsky, E. A. Yelland, A. S. Gibbs, J. A. N. Bruin, M. E. Barber, S. D. Edkins, K. Nishimura, S. Yonezawa, Y. Maeno, and A. P. Mackenzie, Strong increase of T_c of Sr_2RuO_4 under both tensile and compressive strain, Science **344**, 283 (2014).

[25] A. Steppke, L. Zhao, M. E. Barber, T. Scaffidi, F. Jerzembeck, H. Rosner, A. S. Gibbs, Y. Maeno, S. H. Simon, A. P. Mackenzie, and C. W. Hicks, Strong peak in T_c of Sr_2RuO_4 under uniaxial pressure, Science **355**, eaaf9398 (2017).

[26] H.-H. Kim, S. M. Souliou, M. E. Barber, E. Lefrançois, M. Minola, M. Tortora, R. Heid, N. Nandi, R. A. Borzi, G. Garbarino, A. Bosak, J. Porras, T. Loew, M. König, P. J. W. Moll, A. P. Mackenzie, B. Keimer, C. W. Hicks, and M. L. Tacon, Uniaxial pressure control of competing orders in a high-temperature superconductor, Science **362**, 1040 (2018).

[27] H.-H. Kim, E. Lefrançois, K. Kummer, R. Fumagalli, N. B. Brookes, D. Betto, S. Nakata, M. Tortora, J. Porras, T. Loew, M. E. Barber, L. Braicovich, A. P. Mackenzie, C. W. Hicks, B. Keimer, M. Minola, and M. Le Tacon, Charge density waves in $YBa_2Cu_3O_{6.67}$ probed by resonant X-ray scattering under uniaxial compression, Phys. Rev. Lett. **126**, 037002 (2021).

[28] I. Vinograd, S. M. Souliou, A. A. Haghighirad, T. Lacmann, Y. Caplan, M. Frachet, M. Merz, G. Garbarino, Y. Liu, S. Nakata, K. Ishida, H. M. L. Noad, M. Minola, B. Keimer, D. Orgad, C. W. Hicks, and M. Le Tacon, Using strain to uncover the interplay between two- and three-dimensional charge density waves in high-temperature superconducting $YBa_2Cu_3O_y$, Nat. Commun. **15**, 3277 (2024).

[29] A. Najev, S. Hameed, D. Gautreau, Z. Wang, J. Joe, M. Požek, T. Birol, R. M. Fernandes, M. Greven, and D. Pelc, Uniaxial strain control of bulk ferromagnetism in rare-earth titanates, Phys. Rev. Lett. **128**, 167201 (2022).

[30] H.-H. Kim, K. Ueda, S. Nakata, P. Wochner, A. Mackenzie, C. Hicks, G. Khaliullin, H. Liu, B. Keimer, and M. Minola,

Giant stress response of terahertz magnons in a spin-orbit Mott insulator, Nat. Commun. **13**, 6674 (2022).

[31] J. Mutch, W.-C. Chen, P. Went, T. Qian, I. Z. Wilson, A. Andreev, C.-C. Chen, and J.-H. Chu, Evidence for a strain-tuned topological phase transition in ZrTe$_5$, Sci. Adv. **5**, eaav9771 (2019).

[32] See Supplemental Material at http://link.aps.org/supplemental/10.1103/PhysRevB.110.035120 for the sample growth, determination of the real strain, details of the DFT calculations, how the in-house and synchrotron XRD is performed, and the relevant XRD data, which includes Refs. [35–38,49–54].

[33] W. Hayes and R. Loudon, *Scattering of Light by Crystals* (John Wiley and Sons, New York, NY, 1978).

[34] M. Ye, T. Lacmann, M. Frachet, I. Vinograd, G. Garbarino, and A.-A. Haghighirad, Temperature and stress induced structural changes in semiconductor Ta$_2$NiS$_5$ (Version 1) [dataset] (2024) (European Synchrotron Radiation Facility, 2024), doi:10.15151/ESRF-DC-1511921487.

[35] B. Meyer, C. Elsässer, and M. Fähnle, Fortran90 program for mixed-basis pseudopotential calculations for crystals (1997), Max-Planck-Institut für Metallforschung, Stuttgart (unpublished).

[36] J. P. Perdew, K. Burke, and M. Ernzerhof, Generalized gradient approximation made simple, Phys. Rev. Lett. **77**, 3865 (1996).

[37] S. A. Sunshine and J. A. Ibers, Structure and physical properties of the new layered ternary chalcogenides tantalum nickel sulfide (Ta$_2$NiS$_5$) and tantalum nickel selenide (Ta$_2$NiSe$_5$), Inorg. Chem. **24**, 3611 (1985).

[38] R. Heid and K.-P. Bohnen, Linear response in a density-functional mixed basis approach, Phys. Rev. B **60**, R3709 (1999).

[39] A. M. Dadgar, D. Scullion, K. Kang, D. Esposito, E. H. Yang, I. P. Herman, M. A. Pimenta, E.-J. G. Santos, and A. N. Pasupathy, Strain engineering and raman spectroscopy of monolayer transition metal dichalcogenides, Chem. Mater. **30**, 5148 (2018).

[40] M. G. Masteghin, V. Tong, E. B. Schneider, C. C. L. Underwood, T. Peach, B. N. Murdin, R. P. Webb, S. K. Clowes, and D. C. Cox, Stress-strain engineering of single-crystalline silicon membranes by ion implantation: Towards direct-gap group-iv semiconductors, Phys. Rev. Mater. **5**, 124603 (2021).

[41] Z. Peng, X. Chen, Y. Fan, D. J. Srolovitz, and D. Lei, Strain engineering of 2d semiconductors and graphene: from strain fields to band-structure tuning and photonic applications, Light Sci. Appl. **9**, 190 (2020).

[42] J. Cenker, S. Sivakumar, K. Xie, A. Miller, P. Thijssen, Z. Liu, A. Dismukes, J. Fonseca, E. Anderson, X. Zhu, X. Roy, D. Xiao, J.-H. Chu, T. Cao, and X. Xu, Reversible strain-induced magnetic phase transition in a van der waals magnet, Nat. Nanotechnol. **17**, 256 (2022).

[43] N. W. Ashcroft and N. D. Mermin, *Solid State Physics* (Harcourt College Publishers, Orlando, FL, 1976).

[44] H. J. Conley, B. Wang, J. I. Ziegler, R. F. J. Haglund, S. T. Pantelides, and K. I. Bolotin, Bandgap engineering of strained monolayer and bilayer MoS$_2$, Nano Lett. **13**, 3626 (2013).

[45] Y. Y. Hui, X. Liu, W. Jie, N. Y. Chan, J. Hao, Y.-T. Hsu, L.-J. Li, W. Guo, and S. P. Lau, Exceptional tunability of band energy in a compressively strained trilayer MoS$_2$ sheet, ACS Nano **7**, 7126 (2013).

[46] S. Mor, M. Herzog, D. Golež, P. Werner, M. Eckstein, N. Katayama, M. Nohara, H. Takagi, T. Mizokawa, C. Monney, and J. Stähler, Ultrafast electronic band gap control in an excitonic insulator, Phys. Rev. Lett. **119**, 086401 (2017).

[47] S. Mor, M. Herzog, J. Noack, N. Katayama, M. Nohara, H. Takagi, A. Trunschke, T. Mizokawa, C. Monney, and J. Stähler, Inhibition of the photoinduced structural phase transition in the excitonic insulator Ta$_2$NiSe$_5$, Phys. Rev. B **97**, 115154 (2018).

[48] H. M. Bretscher, P. Andrich, P. Telang, A. Singh, L. Harnagea, A. K. Sood, and A. Rao, Ultrafast melting and recovery of collective order in the excitonic insulator Ta2NiSe5, Nat. Commun. **12**, 1699 (2021).

[49] D. Vanderbilt, Optimally smooth norm-conserving pseudopotentials, Phys. Rev. B **32**, 8412 (1985).

[50] Rigaku Oxford Diffraction Ltd., Yarnton, Oxfordshire, E 2015 CrysAlis PRO.

[51] N. Maraytta, P. Nagel, F. Ghorbani, S. Pakhira, A. Ghiami, M. Le Tacon, S. Schuppler, A.-A. Haghighirad, and M. Merz (unpublished).

[52] G. M. Sheldrick, A short history of *SHELX*, Acta Crystallogr. Sec. A **64**, 112 (2008).

[53] G. M. Sheldrick, Crystal structure refinement with *SHELXL*, Acta Crystallogr. Sec. C **71**, 3 (2015).

[54] V. Petříček, M. Dušek, and L. Palatinus, Crystallographic computing system JANA2006: General features, Zeitschrift für Kristallographie (Crystal. Mater.) **229**, 345 (2014).